scientific reports

Check for updates

OPEN

Magnetic UiO-66 functionalized with 4,4′-diamino-2,2′-stilbened isulfonic as a highly recoverable acid catalyst for the synthesis of 4*H*-chromenes in green solvent

Mohammad Reza Khodabakhshi & Mohammad Hadi Baghersad✉

According to 4*H*-chromenes importance, we synthesized a novel magnetic UiO-66 functionalized with 4,4′-diamino-2,2′-stilbenedisulfonic as an efficient and reusable solid acid catalyst for synthesizing 4*H*-chromene skeletons via a one-pot three components reaction in a green solvent. The structure of the synthesized catalyst was confirmed by various techniques including FT-IR, XRD, BET, TGA, TEM, EDX, and SEM, and also the product yields were obtained in 83–96% of yields for all the reactions and under mild conditions. The reported procedure presents an environmentally friendly approach for synthesizing a significant number of 4*H*-chromene derivatives. Correspondingly, MOF-based catalyst makes it easy to separate from reaction media and reuse in the next runs.

4*H*-chromenes can be found in various natural compounds, such as biologically and therapeutically active drugs (anticonvulsants, antimicrobial, and anticancer agents) (Fig. 1)[1]. Researchers have developed several methods for synthesizing 4*H*-chromene derivatives, including using one-pot synthesis methods, recyclable catalysts, green methodologies (reactions in aqueous media), catalyst utilization, and byproduct eliminations[2–6].

Numerous catalytic systems have been developed till today for the synthesis of 4*H*-chromene derivatives, consist of $Fe(HSO4)_3$[7], nickel nanoparticles[8], ZrO_2 nanoparticles[9], $Zn_4O(H_2N\text{-}TA)_3$[10], ZnS nanoparticles[11], nano-sized MgO[12], $CoFe_2O_4$[13], CuO-CeO_2[14], polymer-supported palladacycles[15], [2-aemim][PF_6][16] IL-HSO4@SBA-15[17], SB-DBU.Cl[18], potassiumphthalimide-*N*-oxyl[19], tungstic acid functionalized mesoporous SBA-15[20], heteropolyacid[21], Mg/Al hydrotalcite[22], PEI@Si–MNP[23], PEG-SO_3H[24], alumina[25], nano-sized zeolite clinoptilolite[26], Nickel Nanoparticles[8], $(CTA)_3[SiW_{12}]$-Li^+-MMT[27], PMO-ICS[28], poly(N,N′-dibromo-Nethyl-benzene-1,3-disulfonamide (PBBS)[29], KSF[30], combined NaOAc/KF[31], $MeSO_3H$[32], $TiCl_4$[33,34], MA liquid-phase[35], Bovine Serum Albumin[36], and Cysteic acid grafted to magnetic graphene oxide[37].

However, some of the catalysts for the synthesis of 4*H*-chromenes suffer from disadvantages such as making pollution, having high cost, having difficulty in removing catalysts, and demanding harsh reaction conditions. According to the importance and the broad application of *4H*-chromenes, there is still a great demand for a more feasible, simple, green, and efficient way to synthesize these compounds. For these reasons, we try to design heterogeneous magnetic catalysts to synthesize 4*H*-chromenes with MOFs substrate.

Porous coordination polymers (PCPs), also known as metal–organic frameworks (MOFs), have attracted many scientists' attention during recent years[38–43]. The structure of MOFs can be revised and planned in many ways, considering three main factors: clusters of metal ions, inorganic metal ions, and organic linkers[44–47]. Researchers have designed, synthesized, and commercialized novel MOFs and studied their applications for the last two decades[48–54]. Since MOFs have significant advantages, such as adjustable pore size and functionalities, appropriate capacity for adsorption, considerable specific surface area, and low density, controllable pore functionalities, they can be widely used for adsorption and removal of dyes[55–57].

Nevertheless, some MOFs showed vital negative points, like poor chemical stability. These negative points lead to various limitations in using MOFs' possibilities. To overcome the negative points of MOFs', various functional materials were combined to enhance their ability[58–61]. The synthesis of hybrid nanomaterials based on magnetic nanoparticles and MOFs[62] are of these combinations. These kinds of combinations make it possible to use the

Applied Biotechnology Research Center, Baqiyatallah University of Medical Sciences, Tehran, Iran. ✉email: Hadibaghersad@bmsu.ac.ir

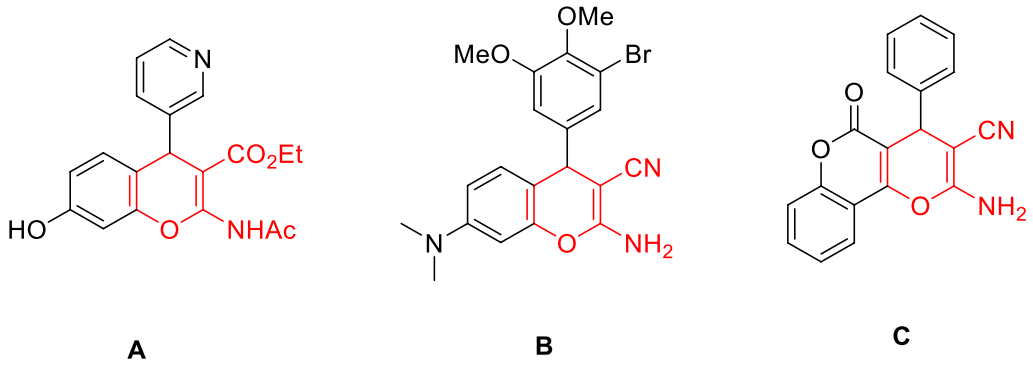

Figure 1. Structures of some biological active 4*H*-chromenes.

advantages of both components, such as high chemical stability and simple separation process, for different applications, especially enhancements in the kinetics of adsorption[63–66].

In detail, magnetic nanomaterials can act as effective adsorbents due to their ease of removing contaminants from wastewater by an applied magnetic field. Also, bio-sorbents have a synergistic effect with their efficient adsorption capacity to remove contaminants, to participate in waste minimization[67,68], and to aid alleviate ecological complications[69]. For these reasons, resulted MOFs from these combinations possess interesting characteristics that could work adequately in CO_2 carbon capture. But the main disadvantage of using MOFs as adsorbents in CO_2 carbon capture is the energy-intensive nature connected with the desorption progression (sunlight, as a powerful external stimulus, can enable the desorption progression with much lesser energy demand over MOF materials). In these occasions, computational screening modeling approaches are influential tools to find optimum performing materials. With the aid of computational modeling, synthesized Mg-IRMOF-74-III showed a CO_2 adsorption capacity of 89.6 $cm^3\ g^{-1}$, which is the highest CO_2 adsorption value within photo-responsive MOFs compared to the reported literatures[70].

As mentioned above, due to magnetic nanoparticles' efficiency, the disadvantage of MOFs could vanish by various methods, like combining the MOFs and magnetic particles. Magnetic hybrid MOFs presented sizeable specific surface areas for their easy separation method. Several methods have been studied till today for the synthesis of magnetic MOFs. These methods include combining the MOFs with Fe_3O_4 by a simple method, coating MOFs onto Fe_3O_4 using layer-by-layer strategy, embedding Fe_3O_4 into MOFs, and encapsulating Fe_3O_4 into MOFs[71–79]. Among all the methods, synthesizing magnetic MOFs using a step-by-step method is one of the most reliable ways. The adjustability of the thickness of the outer shell MOFs is one of the main advantages of this method. Some adjustments are required to develop the compatibility of shell and core and gain the best results[80].

Stilbenes are a class of secondary metabolites containing a trans/cis-ethene double bond and a phenyl on each of the double-bond carbon atoms. The majority of stilbenes are thermally-chemically stable. Additionally, they show fluorescence properties and absorption abilities[81,82]. They play in many required fields such as biomedical[71], biophysical[67], and photochemical research[63]. Due to their applications in a wide range of branches, stilbenes can be used in multidisciplinary fields and syndicates biology, medicine, physics, and chemistry together[83–86]. They are promising agents for use as a functional group for catalytic uses. As the other derivatives of aromatic sulfonic acids, stilbene sulfonic acids are also used to prepare optical brighteners and synthetic dyes[87,88].

In this project, to investigate the applications of recoverable solid acid catalysts for the synthesis of 4*H*-chromenes, Zr clusters with 4,4′-Diamino-2,2′-stilbenedisulfonic were used to design modified magnetic MOF. Zr-cluster-based MOFs, like UiO-66 and UiO-67, have fascinating acid, thermal, and aqueous stabilities[89–94]. Due to their wide range of applications, we have synthesized UiO-66 (Figs. 2, 3) to study its application as a catalyst[95–97] in the synthesis of 4*H*-chromene skeletons via a one-pot three components reaction. The product yields were obtained in 83–96% of yields for all reactions. Studies showed that acidic reagent plays the main role in the catalytic cycle in these reactions.

Results and discussion

The Fe_3O_4@UiO@DAS catalyst was synthesized using a few steps presented in Fig. 2. Details of the preparation method are described in the experimental section.

The FTIR spectrum of Fe_3O_4 (Fig. 4a), Fe_3O_4@UiO-66 can be seen in Fig. 4b. In this figure, the Fe–O band is appeared at 630 cm^{-1} (due to the presence of Fe_3O_4), two peaks at around 1088 cm^{-1} are due to the presence of S–O (stretching vibrations), the peak at 1634 and 1709 cm^{-1} is attributed to C=C and C=O bands, respectively, the C–H bands can be seen at 2931 cm^{-1}, and the strong broad bands at 3435 cm^{-1} can be assigned to stretching of O–H (for Fe_3O_4).

In the spectra of final product Fe_3O_4@UiO@DAS in Fig. 4c, in addition of mentioned peaks for Fe_3O_4@UiO-66, C–N peaks at 1502 and 1573 cm^{-1} can be seen. Also, aromatic peaks are appeared below 1000 cm^{-1}.

In the XRD analysis of Fe_3O_4@UiO@DAS (Fig. 5), observed diffraction peaks are similar to UiO-66 pattern which was reported before[98–100]. In this pattern, not any apparent variations in the characteristic diffraction pattern of Fe_3O_4@UiO-66 were observed. This shows that after growing on the surface of functionalized Fe_3O_4 nanoparticles, the crystalline structure of the MOF was remained unchanged[99,100].

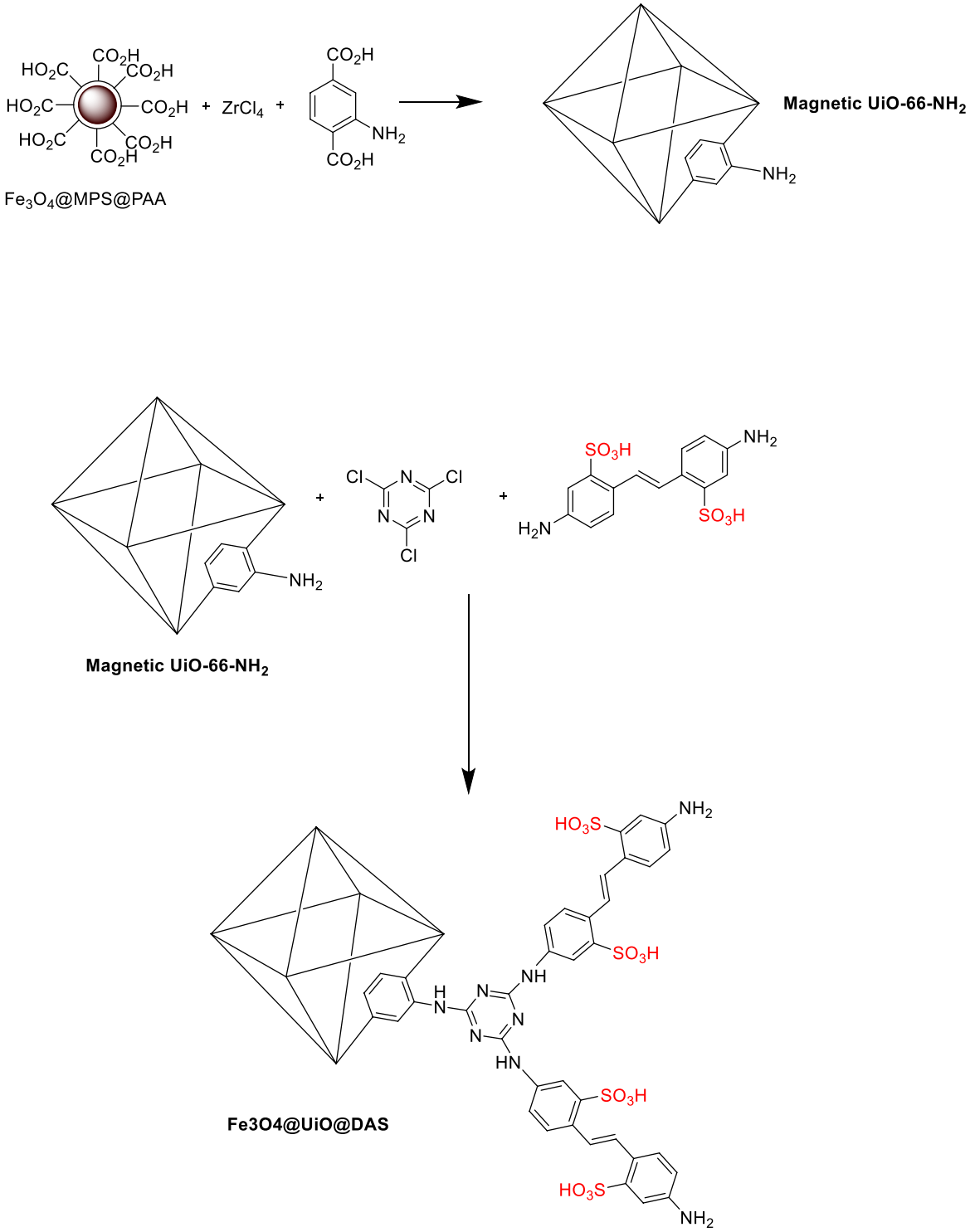

Figure 2. The Synthesis procedure of the Fe_3O_4@UiO@DAS.

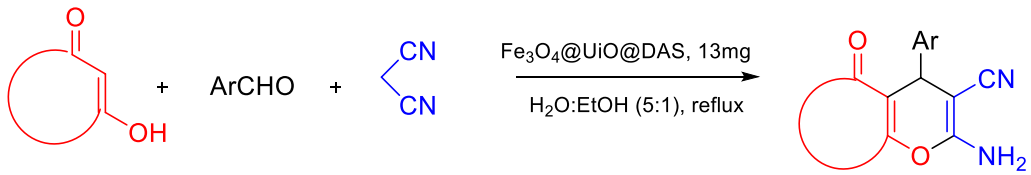

Figure 3. Synthesis of 4*H*-Chromene derivatives catalyzed by Fe_3O_4@UiO@DAS.

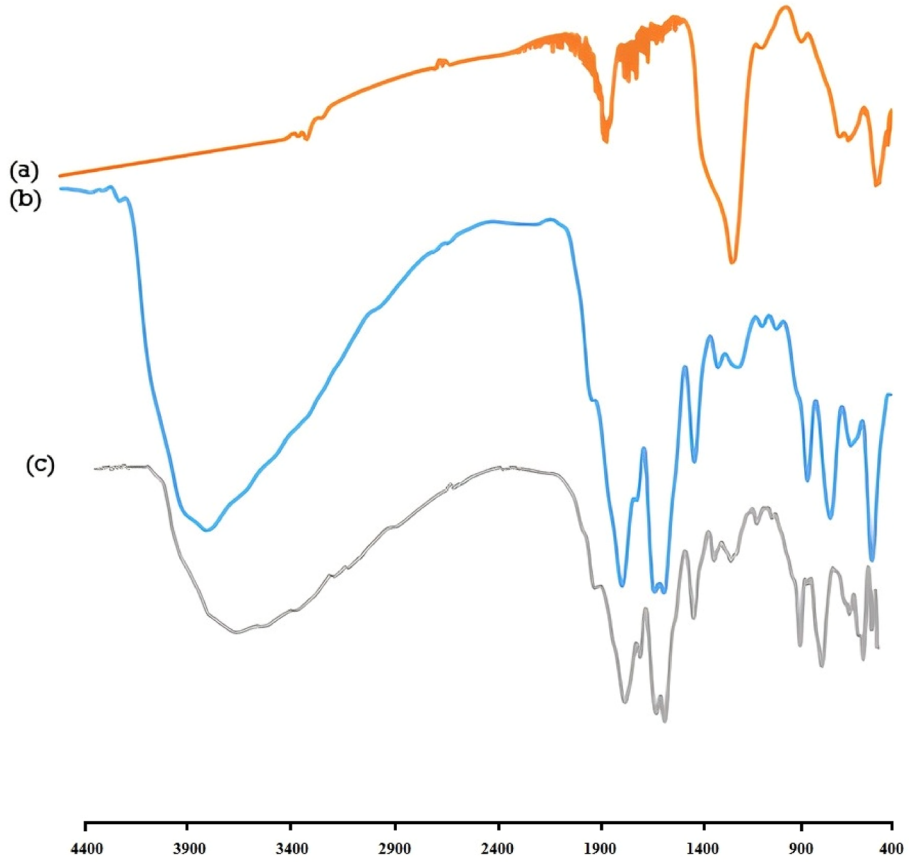

Figure 4. (**a**–**c**) The FTIR spectrums.

To study the morphology, size, and also structure of Fe_3O_4@UiO@DAS, SEM and TEM analyses were used (Figs. 6, 7, 8). The SEM images can show the particle size (by randomly selected particles and studying the size distribution of them) and also illustrated that the particles have a cubic structure. TEM images of the prepared MOF show good agreement with other literatures and can confirm the Fe_3O_4 core of the obtained catalyst. Additionally, using the EDX pattern of the synthesized catalyst, the main elements in its structure (Fe, O, C, N, S) could be understood. These analyses proved the successful synthesis of our catalyst. From EDX we can understand the different amount of carbon in our final catalyst (around 30 weights % in Fe_3O_4@UiO@DAS) from our initial samples.

TGA analysis shows the thermal stability of the synthesized catalyst (Fig. 9). The first decomposition was placed between 100 and 200 °C, due to the trapped water. The second stage, between 260 and 330 °C, is attributed to the decomposition of 4,4′-diamino-2,2′-stilbenedisulfonic acid. Next, the other weight losses that occurred at around 350–390 and 400–420 °C, are because of the removal of hydroxyl, sulfonic acid, and carboxylic acid groups. In higher degrees, owing to the presence of Fe_3O_4, the line becomes stable with no considerable changes.

The N_2 adsorption–desorption data have been summarized in Table 1. The BET specific surface areas of magnetic Fe_3O_4@UiO-66 and Fe_3O_4@UiO@DAS are 828 and 725 $m^2\ g^{-1}$, respectively.

The catalytic ability of the synthesized catalyst was studied through the synthesis of 4*H*-chromene derivatives. To find the optimum reaction condition, the reaction of benzaldehyde (1.0 mmol) (**1**), malononitrile (1.1 mol) (**2**), and 4-hydroxy-6-methyl-2*H*-pyran-2-one (1.0 mmol) (**3**) were studied in various conditions (Table 2). First, different solvents include H_2O, EtOH, EtOH (1):H_2O (5), and THF in the absence of the catalyst. The best yield (29%) was belonged to EtOH (1):H_2O (5) combination (29% yield, 6 h) (Table 2, entries 1–4). Based on the literature, the result shows that a catalyst is necessary to improve the desired reaction rate and yield.

Next, diverse catalysts (4,4′-diamino-2,2′-stilbenedisulfonic acid, MNP@MPS, MNP@MPS@PAA, and Fe_3O_4@UiO-66-NH_2) were used, and the best results were gained using 4,4′-Diamino-2,2′-stilbenedisulfonic acid (73% yield, reflux) (Table 2, entry 5–8).

After that, our synthesized catalyst Fe_3O_4@UiO@DAS was used. The best result was gained in the existence of 5 mg of catalyst (68% yield, reflux, 0.5 h) (Table 2, entries 8–13). By studying the amount of catalyst, it was understood that in the presence of 13 mg of the catalyst, the yield of 94% could be gained at 30 min (Table 2, entries 15). By increasing the catalyst amount from 13 to 15 mg, no change in reaction yield was observed (Table 2, entries 16). This result clearly shows that Fe_3O_4@UiO@DAS effectively improves the reaction yield. The acidic functional groups (SO_3H) of 4,4′-diamino-2,2′-stilbenedisulfonic acid as Bronsted acids improve the reaction yield and the nano-particles can also race the reaction up as Lewis acids. However, the optimization

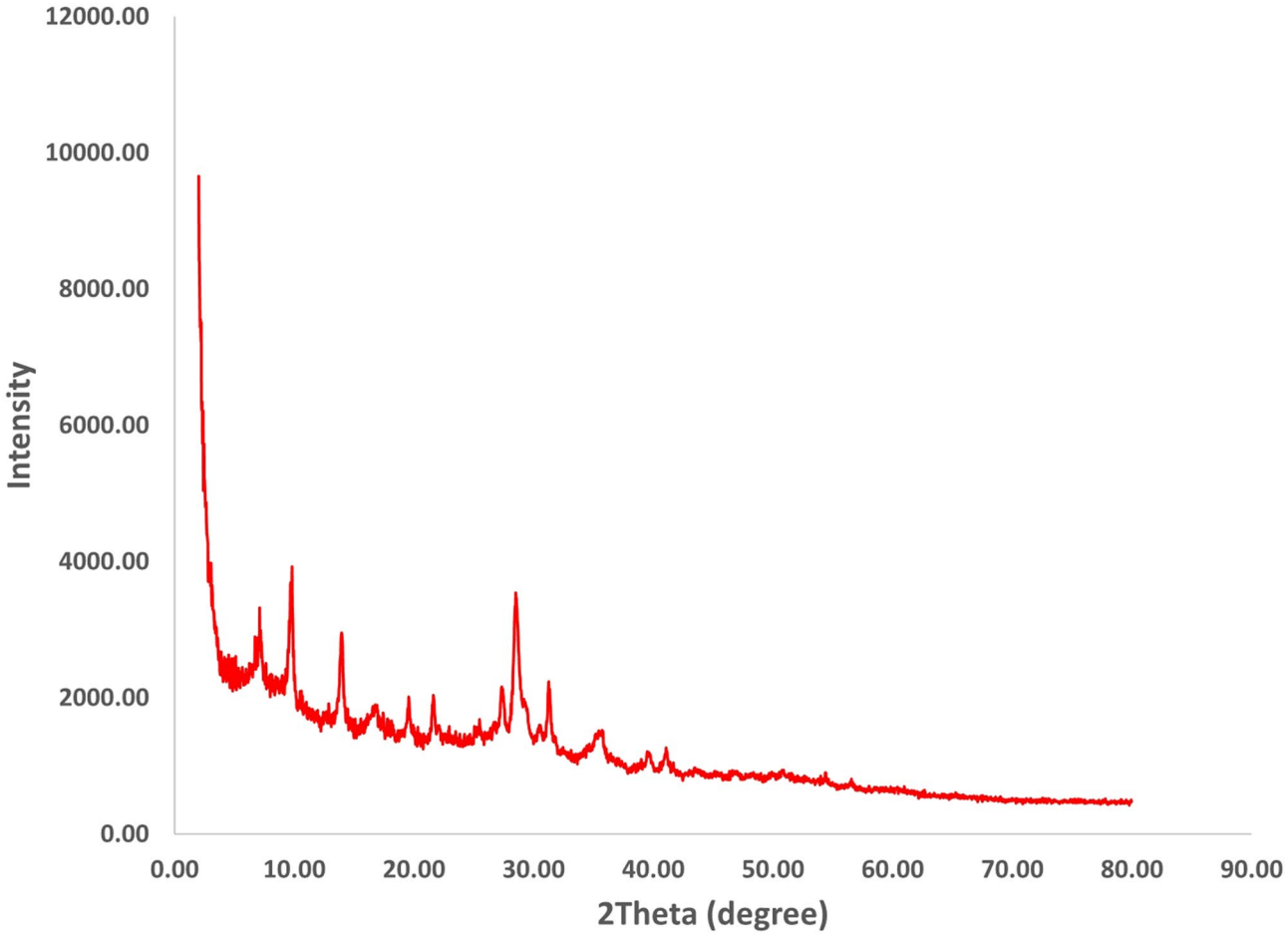

Figure 5. XRD pattern of Fe_3O_4@UiO@DAS.

results indicate the major active site of the nano-particles to be disulfonic acid functional groups. It should be noted that in all reactions, the catalyst was separated by an external magnet and the final products were filtered out of the mixture.

Additionally, we developed the optimized reaction condition (13 mg of Fe_3O_4@UiO@DAS in 3 ml of water–ethanol (5:1) under reflux conditions) for other derivatives of aromatic aldehydes (**1**) and 4-hydroxy-6-methyl-2H-pyran-2-one, 4-hydroxy coumarin and dimedone compound (**3**, **4**, **7**) for the synthesis of the various derivatives of 4*H*-chromenes (**5a–i**, **6a–i**, **8a–h**). The results have been presented in Tables 3, 4 and 5.

Optimized reaction condition also was for the synthesis of 2-amino-7,7-dimethyl-5-oxo-4-aryl-5,6,7,8-tetrahydro-4*H*-chromene-3-carbonitrile, which were collected in Table 4.

It is noteworthy that in all reactions for the synthesis of 4*H*-chromene derivatives (5, 6, 7) syntheses, the reaction of aromatic aldehydes which possessed electron-withdrawing groups are shown to be faster than the reaction of aromatic aldehydes with electron-donating groups. Dimedone required a shorter reaction time compared to the 4-hydroxy-pyrane and 4-hydroxy-coumarin.

For the importance of using heterogeneous catalysts in industrial processes, recyclability of our synthesized catalyst was studied using optimized reaction conditions for synthesis 2-amino-3-cyano-4*H*-chromene via condensation of benzaldehydes (1a), malononitrile (2), and 4-hydroxy-6-methyl-2H-pyran-2-one (3) in the presence of 13 mg of Fe_3O_4@UiO@DAS. Our gained results (Table 6) could be used 7 times without a dramatic decrease in its ability. After each reaction, the catalyst was separated by an external magnetic field and washed twice with hot deionized water (10 mL), once with 10 mL ethanol, dried in an oven at 60 °C for 24 h in a vacuum oven reused in the model reaction.

Experimental

Materials. Our initial materials were provided from Merck and Sigma companies ($FeCl_2.4H_2O$, $FeCl_3.6H_2O$, DMF, NH_4OH, terephthalic acid, 3-methacryloxypropyltrimethoxy silane (MPS), 4,4′-diaminostilbene-2,2′-disulfonic acid (DAS), Zirconium (IV) chloride, 2,2′-azobisisobutyronitrile (AIBN), and Cyanuric chloride were obtained from Sigma-Aldrich without any purification. The monomer of acrylic acid was supplied by Sigma-Aldrich and was distilled before use.

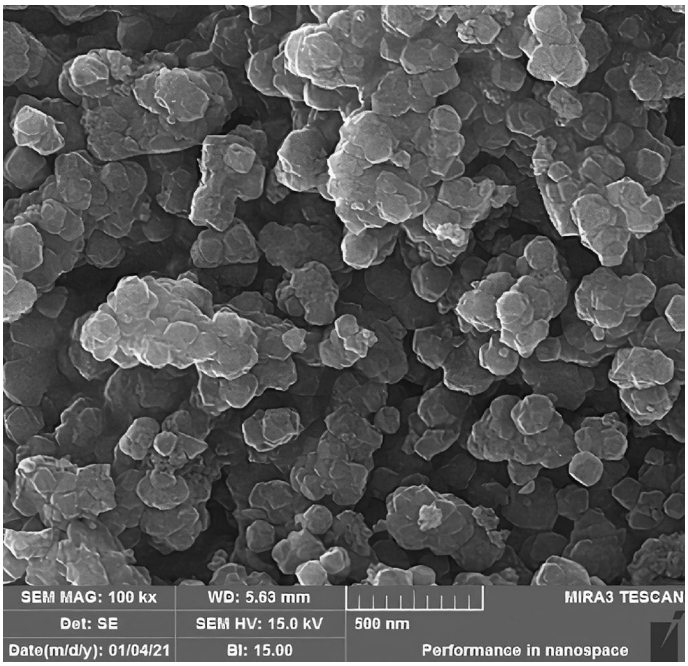

Figure 6. SEM analysis of Fe_3O_4@UiO@DAS.

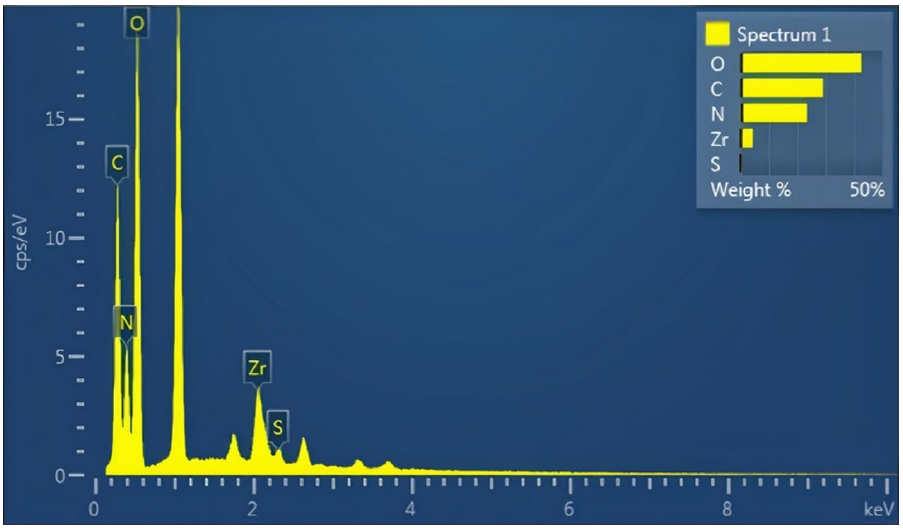

Figure 7. EDX analysis of Fe_3O_4@UiO@DAS.

Preparation of catalyst. The magnetic nanoparticle (Fe_3O_4) was synthesized using the co-precipitation approach[101,102]. After synthesizing it, Fe_3O_4@SiO_2 (1 g) was dispersed in dry EtOH and NH_4OH (2 mL) was added to the mixture. Then, MPS (10 mL) was gradually added to the above mixture at 60 °C, and for 48 h the mixture was stirred. Using an external magnet, magnetic nanoparticles were collected, washed, and dried for 24 h under vacuum conditions.

Next, 0.4 of synthesized magnetic nanoparticles (which we called MNP@MPS) was dispersed in MeOH (30 mL), and acrylic acid (0.4 g) was added to it. After purging Ar into the mixture (for 20 min), AIBN (0.1) was added to it and the mixture was stirred for 24 h at 70 °C. The final product (MNP@PAA) was collected by an external magnet, washed, and dried under vacuum conditions.

To synthesize of Fe_3O_4@UiO-66, synthesized MNP@MPS@PAA (0.2 g) was added to DMF (30 mL) and sonicated for 30 min. Next, by adding 0.53 g of zirconium (IV) chloride (0.53 g) and terephthalic acid (0.38 g) to the mixture, it was left to stir for 2 h. after 2 h, the autoclave was used to heat the mixture (120 °C, 1 day).

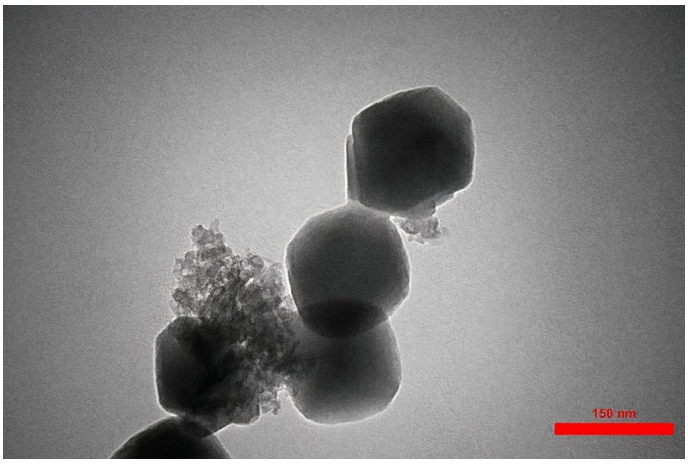

Figure 8. TEM analysis of Fe_3O_4@UiO@DAS.

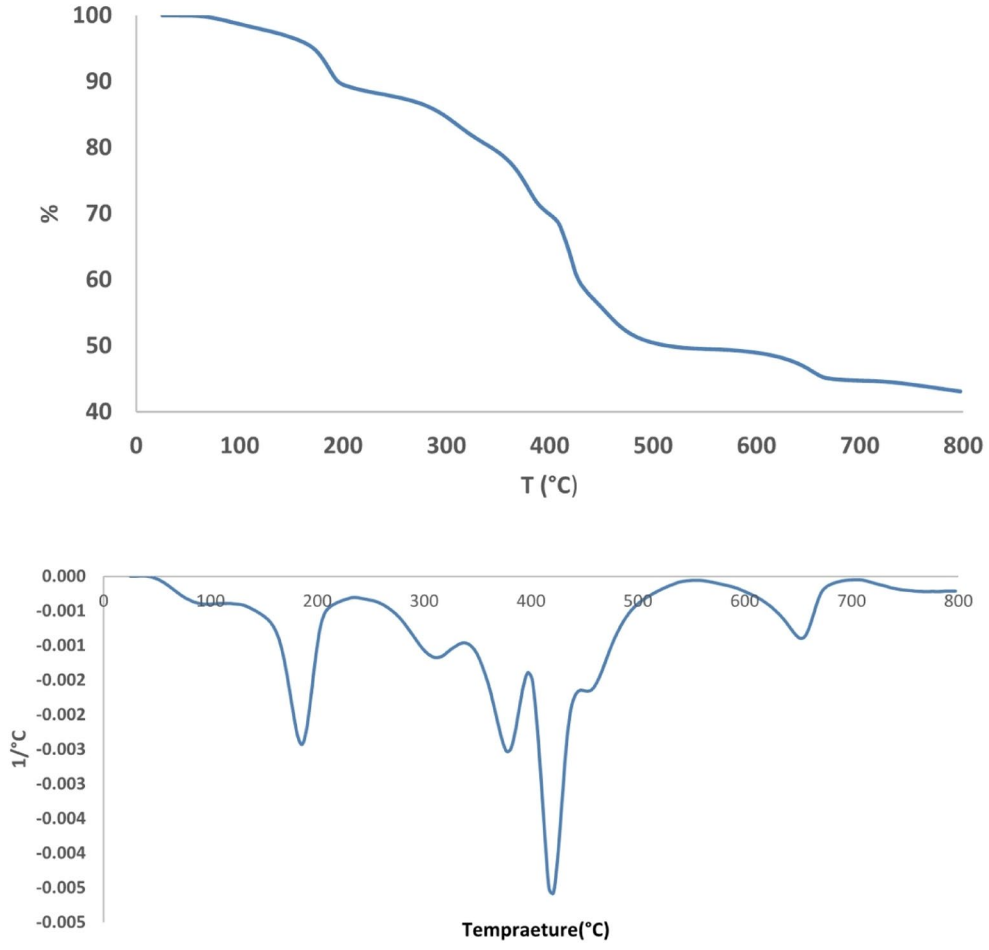

Figure 9. TGA-DTG analysis.

Resulted product was centrifuged and washed. Also, chloroform was used for the exchanging of the solvent. Finally, Magnetic UiO-66-NH_2 was heated to 120 °C and kept under vacuum condition for one week.

To access the final catalyst Fe_3O_4@UiO@DAS, Fe_3O_4@UiO-66-NH_2 (1.0 g) was dispersed in 20 mL of dry THF in a round bottom flask and sonicated for 20 min. Then, TCT (2.0 g, 10 mmol) was added to the mixture. Afterward, 4,4′-diamino-2,2′-stilbenedisulfonic acid (2.9 g, 14 mmol) was added gradually to the mixture under stirring at 0 °C. Then, K_2CO_3 (2.0 g, 14 mmol) was added in the next step to the mixture and stirred for 3–4 h at

Sample	Total pore volume ($cm^3\ g^{-1}$)	BET surface area ($m^2\ g^{-1}$)	Pore diameter (nm)
Fe_3O_4@UiO-66	0.41	828	5.1
Fe_3O_4@UiO@DAS	0.38	725	4.8

Table 1. N_2 adsorption–desorption data.

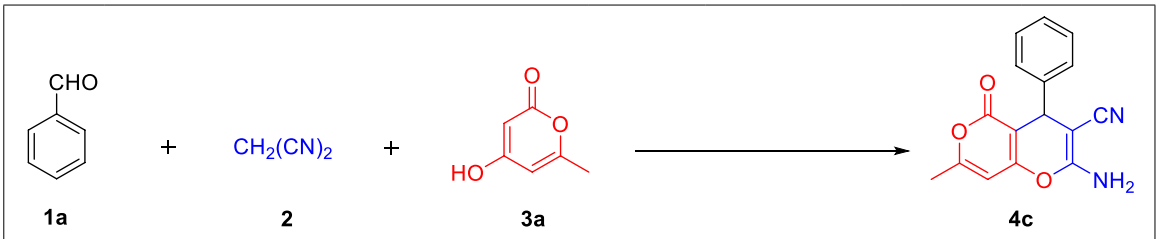

Entry	Cat. (mg)	Temp	Solv	Time (h)	Yield[a] (%)
1	–	Reflux	H_2O	6	18
2	–	Reflux	EtOH	6	21
3	–	Reflux	H_2O:EtOH (5:1)	6	29
4	–	Reflux	THF	6	Trace
5	4,4′-Diamino-2,2′-stilbenedisulfonic acid **3** mg	Reflux	H_2O:EtOH (5:1)	6	73
6	MNP@MPS **3** mg	Reflux	H_2O:EtOH (5:1)	6	32
7	MNP@MPS@PAA **3** mg	Reflux	H_2O:EtOH (5:1)	6	45
8	Fe_3O_4@UiO-66-NH_2 **3** mg	Reflux	H_2O:EtOH (5:1)	6	32
9	Fe_3O_4@UiO@DAS **5** mg	Ambient	Solvent-free	6	Trace
10	Fe_3O_4@UiO@DAS **5** mg	80	Solvent-free	6	57
11	Fe_3O_4@UiO@DAS **5** mg	Reflux	H_2O:EtOH (5:1)	6	65
12	Fe_3O_4@UiO@DAS **5** mg	Reflux	H_2O:EtOH (5:1)	3	65
13	Fe_3O_4@UiO@DAS **5** mg	Reflux	H_2O:EtOH (5:1)	0.5	65
14	Fe_3O_4@UiO@DAS **10** mg	Reflux	H_2O:EtOH (5:1)	0.5	83
15	**Fe_3O_4@UiO@DAS 13 mg**	**Reflux**	**H_2O:EtOH (5:1)**	**0.5**	**94**
16	Fe_3O_4@UiO@DAS 15 mg	Reflux	H_2O:EtOH (5:1)	0.5	94

Table 2. Optimization of the reaction condition for the synthesis of 2-amino-3-cyano-4*H*-chromene catalyzed by Fe_3O_4@UiO@DAS. Reaction conditions: Benzaldehyde (1a, 1 mmol), malononitrile (2, 1.1 mmol), and 4-hydroxy-6-methyl-2*H*-pyran-2-one (3a, 1 mmol) in the presence of Fe_3O_4@UiO@DAS and 2 ml of water–ethanol (5:1) as a green solvent. Significant values are in [bold]. [a]Isolated yields.

room temperature and then was refluxed at 50 °C for 24 h. The prepared Fe_3O_4@UiO-66-NH_2 was magnetically separated and washed three times with methanol and chloroform to remove any excess reagents and then dried at 60 °C for 24 h in a vacuum oven.

Synthesis of 4H-chromene derivatives. A glass vial was successively charged with different enolizable compounds (1 mmol), aldehydes (1 mmol), and active methylene nitrile (1.1 mmol) in the presence of Fe_3O_4@UiO@DAS (13 mg), in water–ethanol (5:1, 3 mL) at reflux temperature. The reaction mixture was stirred for the appropriate time brought in Tables 3, 4, and 5. After reaction completion, which was controlled by Thin Layer Chromatography (TLC) test (using EtOAc/n-Hexane, 1:3 as solvent), the catalyst was separated by a magnet, and the obtained solid product was filtered. In the case of impurities, the obtained product was recrystallized from ethanol.

Conclusions

Zr-cluster-based MOFs have fascinating characteristics and have huge variety of applications. To increase their applications, hybrid nanomaterials based on MOFs have synthesized. Synthesizing hybrid materials make it possible to use the advantages of both parts in their structures. In this project, to use the advantages of MOFs (such as high chemical stability) and magnetic nanoparticles (such as simple separation process) we have decided to synthesize a novel magnetic UiO-66 functionalized with 4,4′-diamino-2,2′-stilbenedisulfonic. This modified MOF characterized by various techniques, including FT-IR, XRD, BET, TGA, TEM, EDX, and SEM. To investigate the applications of our modified magnetic MOF, it was used for the synthesis of 4*H*-chromene skeletons via a one-pot three components reaction in a green solvent. This non-hazardous, recyclable, effective, and appropriate catalyst allowed quick and effective access to diverse 4*H*-chromene derivatives. The synthesized catalyst can

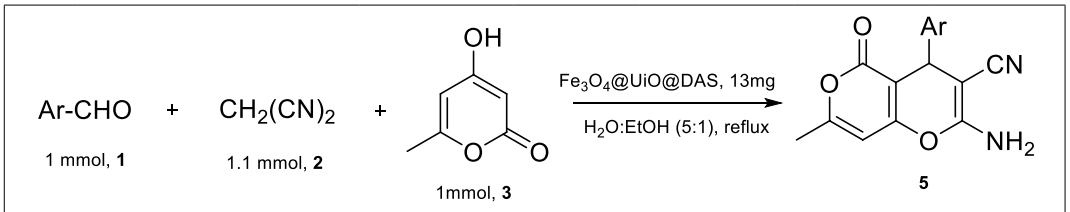

En	Aldehyde	Compound	Product[a]	Time (min)	Yield[b] (%)	M.P (°C)
1	Benzaldehyde	3	5a	30	94	231–233
2	2-Chlorobenzaldehyde	3	5b	20	90	267–269
3	4-Chlorobenzaldehyde	3	5c	20	96	227–229
4	4-Nitrobenzaldehyde	3	5d	15	95	211–213
5	3-Nitrobenzaldehyde	3	5e	15	89	231–232
6	Terephthaldehyde	3	5f	40	83	255–257
7	4-Methoxybenzaldehyde	3	5g	40	90	213–215
8	4-Ethoxybenzaldehyde	3	5h	40	90	202–204
9	3-Methylbenzaldehyde	3	5i	40	89	232–234

Table 3. Three-component synthesis of different 2-amino-7-methyl-5-oxo-4-phenyl-4,5-dihydropyrano[4,3-*b*] pyran-3-carbonitrile (5a-i) via condensation of various aldehydes (1), malononitrile (2) and 4-hydroxy-6-methyl-2*H*-pyran-2-one (3) in the presence of Fe_3O_4@UiO@DAS. Reaction conditions: Aldehyde (1, 1 mmol), Malononitrile (2, 1.1 mmol), 4-hydroxy-6-methyl-2*H*-pyran-2-one (3) (1 mmol), and Fe_3O_4@UiO@DAS (13 mg) at reflux conditions. [a]All compounds are known and their structures were established from their melting points compared with authentic samples or literature values. [b]Isolated yield

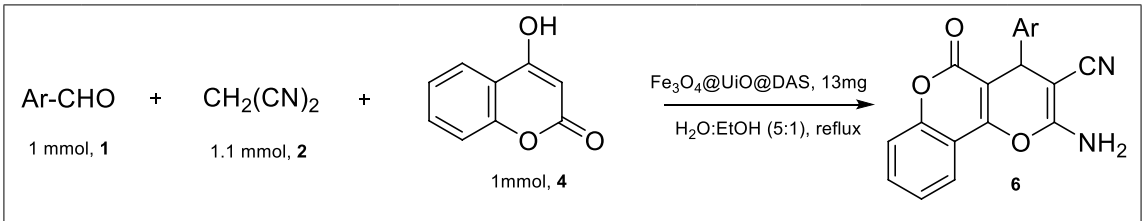

En	Aldehyde	Compound	Product[a]	Time (min)	Yield[b] (%)	M.P (°C)
1	Benzaldehyde	4	6a	30	91	256–258
2	4-Chlorobenzaldehyde	4	6b	30	93	255–257
3	2,4-Dichlorobenzaldehyde	4	6c	30	89	261–263
4	4-Nitrobenzaldehyde	4	6d	15	89	254–256
5	3-Nitrobenzaldehyde	4	6e	15	89	256–259
6	4-Methylbenzaldehyde	4	6f	40	95	250–252
7	3-Methylbenzaldehyde	4	6g	40	89	253–255
8	4-Methoxybenzaldehyde	4	6h	40	93	233–235
9	Terephthaldehyde	4	6i	40	85	297–299

Table 4. Three-component synthesis of different 2-amino-5-oxo-4-phenyl-4,5-dihydropyrano[3,2-*c*] chromene-3-carbonitrile (6a–i) via condensation of various aldehydes (1), malononitrile (2), and 4-hydroxy coumarin (4) in the presence of Fe_3O_4@UiO@DAS. Reaction conditions: Aldehyde (1, 1 mmol), Malononitrile (2, 1.1 mmol), 4-hydroxy coumarin (4) (1 mmol), and Fe_3O_4@UiO@DAS (13 mg) at reflux conditions. [a]All compounds are known and their structures were established from their melting points compared with authentic samples or literature values. [b]Isolated yield.

be extracted from the reaction media by an external magnetic field and recycled. Briefly, the absence of harsh conditions in the synthesis of catalyst, reusability, mild reaction conditions, and up to 96% yields of products are advantageous of our introduced method.

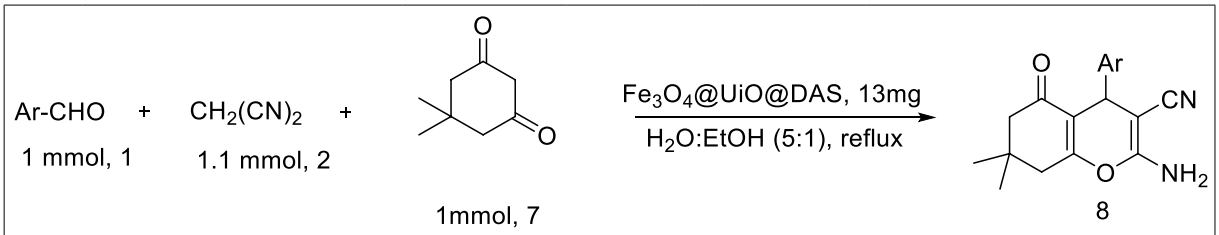

En	Aldehyde	Compound	Product[a]	Time (min)	Yield[b] (%)	M.P (°C) Obsd
1	Benzaldehyde	7	8a	20	91	235–237
2	2-Chlorobenzaldehyde	7	8b	20	93	218–220
3	4-Methoxybenzaldehyde	7	8c	25	90	212–214
4	4-Methylbenzaldehyde	7	8d	25	90	196–198
5	2,4-Dichlorobenzaldehyde	7	8e	20	88	221–223
6	Terphthaldehyde	7	8f	30	90	206–208
7	3-Nitrobenzaldehyde	7	8g	15	86	210–211
8	2-Nitrobenzaldehyde	7	8h	15	86	218–220

Table 5. Three-component synthesis of different 4*H*-chromene (8a–h) via condensation of various aldehydes (1), malononitrile (2) and dimedone (7) in the presence of Fe_3O_4@UiO@DAS. Reaction conditions: Aldehyde (1, 1 mmol), Malononitrile (2, 1.1 mmol), dimedone (7, 1 mmol), and Fe_3O_4@UiO@DAS (13 mg) at reflux conditions. [a]All compounds are known and their structures were established from their melting points compared with authentic samples or literature values. [b]Isolated yield.

Cycle	1	2	3	4	5	6	7
Yield %	94	94	92	92	89	89	88

Table 6. Recyclability of synthesized Fe_3O_4@UiO@DAS for synthesis 2-amino-3-cyano-4H-chromene via condensation of benzaldehydes (1a), malononitrile (2) and 4-hydroxy-6-methyl-2*H*-pyran-2-one (3) in the presence of Fe_3O_4@UiO@DAS.

Received: 21 December 2021; Accepted: 14 March 2022
Published online: 01 April 2022

References

1. Raj, V. & Lee, J. 2H/4H-chromenes—A versatile biologically attractive scaffold. *Front. Chem.* **8**, 623 (2020).
2. Heravi, M. R. P., Aghamohammadi, P. & Vessally, E. Green synthesis and antibacterial, antifungal activities of 4H-pyran, tetrahydro-4H-chromenes and spiro2-oxindole derivatives by highly efficient Fe_3O_4@ SiO2@ NH_2@ Pd $(OCOCH3)_2$ nanocatalyst. *J. Mol. Struct.* **1249**, 131534 (2022).
3. González-Rodal, D., Palomino, G. T., Cabello, C. P. & Pérez-Mayoral, E. Amino-grafted Cu and Sc metal-organic frameworks involved in the green synthesis of 2-amino-4H-chromenes. Mechanistic understanding. *Microporous Mesoporous Mater.* **323**, 111232 (2021).
4. Das, D. Ascorbic acid: an efficient organocatalyst for environmentally benign synthesis of indole-substituted 4H-chromenes. *Monatshefte für Chemie-Chem. Monthly* **152**, 987–991 (2021).
5. Babaei, P. & Safaei-Ghomi, J. L-Proline covered N doped graphene quantum dots modified CuO/ZnO hexagonal nanocomposite as a robust retrievable catalyst in synthesis of substituted chiral 2-amino-4H-chromenes. *Mater. Chem. Phys.* **267**, 124668 (2021).
6. Kantharaju, K. & Khatavi, S. Y. Microwave accelerated synthesis of 2-amino-4H-chromenes catalyzed by WELFSA: A green protocol. *ChemistrySelect* **3**, 5016–5024 (2018).
7. Sonsona, I. G., Marqués-López, E. & Herrera, R. P. Enantioselective organocatalyzed synthesis of 2-amino-3-cyano-4H-chromene derivatives. *Symmetry* **7**, 1519–1535 (2015).
8. Khurana, J. M. & Vij, K. Nickel nanoparticles as semiheterogeneous catalyst for one-pot, three-component synthesis of 2-amino-4*H*-pyrans and pyran annulated heterocyclic moieties. *Synth. Commun.* **43**, 2294–2304 (2013).
9. Bodhak, C., Kundu, A. & Pramanik, A. ZrO_2 nanoparticles as a reusable solid dual acid–base catalyst for facile one-pot synthesis of multi-functionalized spirooxindole derivatives under solvent free condition. *RSC Adv.* **5**, 85202–85213 (2015).
10. Rostamnia, S. & Morsali, A. Size-controlled crystalline basic nanoporous coordination polymers of Zn_4O(H2N-TA)3: Catalytically study of IRMOF-3 as a suitable and green catalyst for selective synthesis of tetrahydro-chromenes. *Inorg. Chim. Acta* **411**, 113–118 (2014).
11. Dandia, A., Parewa, V., Jain, A. K. & Rathore, K. S. Step-economic, efficient, ZnS nanoparticle-catalyzed synthesis of spirooxindole derivatives in aqueous medium via Knoevenagel condensation followed by Michael addition. *Green Chem.* **13**, 2135–2145 (2011).
12. Kumar, D. *et al.* Nanosized magnesium oxide as catalyst for the rapid and green synthesis of substituted 2-amino-2-chromenes. *Tetrahedron* **63**, 3093–3097 (2007).
13. Rajput, J. K. & Kaur, G. Synthesis and applications of $CoFe_2O_4$ nanoparticles for multicomponent reactions. *Catal. Sci. Technol.* **4**, 142–151 (2014).

14. Albadi, J., Razeghi, A., Mansournezhad, A. & Azarian, Z. CuO–CeO_2 nanocomposite catalyzed efficient synthesis of amino-chromenes. *J. Nanostruct. Chem.* **3**, 85 (2013).
15. Hershberger, J. C., Zhang, L., Lu, G. & Malinakova, H. C. Polymer-supported palladacycles: Efficient reagents for synthesis of Benzopyrans with palladium recovery relationship among resin loading, Pd:P ratio, and reactivity of immobilized palladacycles. *J. Organ. Chem.* **71**, 231–235 (2006).
16. Peng, Y. & Song, G. Amino-functionalized ionic liquid as catalytically active solvent for microwave-assisted synthesis of 4H-pyrans. *Catal. Commun.* **8**, 111–114 (2007).
17. Rostamnia, S., Hassankhani, A., Hossieni, H. G., Gholipour, B. & Xin, H. Brønsted acidic hydrogensulfate ionic liquid immobilized SBA-15:[MPIm][HSO4]@ SBA-15 as an environmentally friendly, metal-and halogen-free recyclable catalyst for Knoevenagel–Michael-cyclization processes. *J. Mol. Catal. A Chem.* **395**, 463–469 (2014).
18. Hasaninejad, A., Golzar, N., Beyrati, M., Zare, A. & Doroodmand, M. M. Silica-bonded 5-n-propyl-octahydro-pyrimido[1,2-a] azepinium chloride (SB-DBU)Cl as a highly efficient, heterogeneous and recyclable silica-supported ionic liquid catalyst for the synthesis of benzo[b]pyran, bis(benzo[b]pyran) and spiro-pyran derivatives. *J. Mol. Catal. A: Chem.* **372**, 137–150 (2013).
19. Dekamin, M. G., Eslami, M. & Maleki, A. Potassium phthalimide-*N*-oxyl: A novel, efficient, and simple organocatalyst for the one-pot three-component synthesis of various 2-amino-4*H*-chromene derivatives in water. *Tetrahedron* **69**, 1074–1085 (2013).
20. Kundu, S. K., Mondal, J. & Bhaumik, A. Tungstic acid functionalized mesoporous SBA-15: A novel heterogeneous catalyst for facile one-pot synthesis of 2-amino-4*H*-chromenes in aqueous medium. *Dalton Trans.* **42**, 10515–10524 (2013).
21. Heravi, M. M., Bakhtiari, K., Zadsirjan, V., Bamoharram, F. F. & Heravi, O. M. Aqua mediated synthesis of substituted 2-amino-4*H*-chromenes catalyzed by green and reusable Preyssler heteropolyacid. *Bioorg. Med. Chem. Lett.* **17**, 4262–4265 (2007).
22. Kale, S. R., Kahandal, S. S., Burange, A. S., Gawande, M. B. & Jayaram, R. V. A benign synthesis of 2-amino-4H-chromene in aqueous medium using hydrotalcite (HT) as a heterogeneous base catalyst. *Catal. Sci. Technol.* **3**, 2050–2056 (2013).
23. Hamadi, H., Gholami, M. & Khoobi, M. Polyethyleneimine-modified super paramagnetic Fe_3O_4 nanoparticles: An efficient, reusable and water tolerance nanocatalyst. *Int. J Heterocycl. Chem.* **1**(3), 23–34 (2011).
24. Shitole, N. V., Shelke, K. F., Sadaphal, S. A., Shingate, B. B. & Shingare, M. S. PEG-400 remarkably efficient and recyclable media for one-pot synthesis of various 2-amino-4*H*-chromenes. *Green Chem. Lett. Rev.* **3**, 83–87 (2010).
25. Maggi, R., Ballini, R., Sartori, G. & Sartorio, R. Basic alumina catalysed synthesis of substituted 2-amino-2-chromenes via three-component reaction. *Tetrahedron Lett.* **45**, 2297–2299 (2004).
26. Baghbanian, S. M., Rezaei, N. & Tashakkorian, H. Nanozeolite clinoptilolite as a highly efficient heterogeneous catalyst for the synthesis of various 2-amino-4*H*-chromene derivatives in aqueous media. *Green Chem.* **15**, 3446–3458 (2013).
27. Abbaspour-Gilandeh, E., Aghaei-Hashjin, M., Yahyazadeh, A. & Salemi, H. (CTA)3[SiW12]-Li+-MMT: A novel, efficient and simple nanocatalyst for facile and one-pot access to diverse and densely functionalized 2-amino-4*H*-chromene derivatives via an eco-friendly multicomponent reaction in water. *RSC Adv.* **6**, 55444–55462 (2016).
28. Yaghoubi, A., Dekamin, M. G., Arefi, E. & Karimi, B. Propylsulfonic acid-anchored isocyanurate-based periodic mesoporous organosilica (PMO-ICS-Pr-SO3H): A new and highly efficient recoverable nanoporous catalyst for the one-pot synthesis of bis (indolyl) methane derivatives. *J. Colloid Interface Sci.* **505**, 956–963 (2017).
29. Ghorbani-Vaghei, R. & Malaekehpoor, S. M. N-Bromosulfonamides catalyzed synthesis of new spiro[indoline-3,4′-pyrano [2,3-c] pyrazole] derivatives. *J. Heterocycl. Chem.* **54**, 465–472 (2017).
30. Ballini, R. *et al.* Multicomponent reactions under clay catalysis. *Catal. Today* **60**, 305–309 (2000).
31. Elinson, M. N. *et al.* Solvent-free cascade reaction: direct multicomponent assembling of 2-amino-4*H*-chromene scaffold from salicylaldehyde, malononitrile or cyanoacetate and nitroalkanes. *Tetrahedron* **66**, 4043–4048 (2010).
32. Heravi, M. M., Baghernejad, B. & Oskooie, H. A. A novel and efficient catalyst to one-pot synthesis of 2-amino-4*H*-chromenes by methanesulfonic acid. *J. Chin. Chem. Soc.* **55**, 659–662 (2008).
33. Sunil Kumar, B. *et al.* An efficient approach towards three component coupling of one pot reaction for synthesis of functionalized benzopyrans. *J. Heterocycl. Chem.* **43**, 1691–1693 (2006).
34. Eshghi, H., Damavandi, S. & Zohuri, G. H. Efficient one-pot synthesis of 2-amino-4H-chromenes catalyzed by ferric hydrogen sulfate and Zr-based catalysts of FI. *Synth. Reac. Inorg. Met.-Org. Nano-Met. Chem.* **41**(9), 1067–1073 (2011).
35. Rai, P., Srivastava, M., Singh, J. & Singh, J. Chitosan/ionic liquid forms a renewable and reusable catalyst system used for the synthesis of highly functionalized spiro derivatives. *N. J. Chem.* **38**, 3181–3186 (2014).
36. Dalal, K. S. *et al.* Bovine serum albumin catalyzed one-pot, three-component synthesis of dihydropyrano[2,3-c]pyrazole derivatives in aqueous ethanol. *RSC Adv.* **6**, 14868–14879 (2016).
37. Matloubi Moghaddam, F., Eslami, M. & Hoda, G. Cysteic acid grafted to magnetic graphene oxide as a promising recoverable solid acid catalyst for the synthesis of diverse 4*H*-chromene. *Sci. Rep.* **10**, 20968 (2020).
38. Dutta, S., Let, S., Sharma, S., Mahato, D. & Ghosh, S. K. Recognition and sequestration of toxic inorganic water pollutants with hydrolytically stable metal-organic frameworks. *Chem. Rec.* **21**, 1666–1680 (2021).
39. Zhang, Y. *et al.* Recent progress in lanthanide metal–organic frameworks and their derivatives in catalytic applications. *Inorg. Chem. Front.* **8**, 590–619 (2021).
40. Yin, W., Zhang, G., Wang, X. & Pang, H. One-dimensional metal–organic frameworks for electrochemical applications. *Adv. Colloid Interface Sci.* **298**, 102562 (2021).
41. Ahmadijokani, F. *et al.* UiO-66 metal–organic frameworks in water treatment: A critical review. *Progress Mater. Sci.* **125**, 100904 (2022).
42. Chen, Z. *et al.* Hybrid porous crystalline materials from metal organic frameworks and covalent organic frameworks. *Adv. Sci.* **8**, 2101883 (2021).
43. Abdel Maksoud, M. I. A. *et al.* Engineered magnetic oxides nanoparticles as efficient sorbents for wastewater remediation: A review. *Environ. Chem. Lett.* https://doi.org/10.1007/s10311-021-01351-3 (2021).
44. Cai, W., Liu, X., Wang, L. & Wang, B. Design and synthesis of noble metal-based electrocatalysts using metal-organic frameworks and derivatives. *Mater. Today Nano.* **17**, 100144 (2022).
45. Najafi, M. *et al.* Metal-organic and covalent organic frameworks for the remediation of aqueous dye solutions: Adsorptive, catalytic and extractive processes. *Coordination Chem. Rev.* **454**, 214332 (2022).
46. Lin, R.-B., Zhang, Z. & Chen, B. Achieving high performance metal-organic framework materials through pore engineering. *Acc. Chem. Res.* **54**, 3362–3376 (2021).
47. Fu, J. & Wu, Y. Frontispiece: A showcase of green chemistry: Sustainable synthetic approach of zirconium-based MOF materials. *Chem. Eur. J.* **27**, 9967–9987 (2021).
48. Zhang, Y. *et al.* Construction of UiO-NH2@TiC Schottky junction and their effectively photocatalytic and antibacterial performance. *J. Cluster Sci.* https://doi.org/10.1007/s10876-022-02233-6 (2022).
49. Cao, P. *et al.* Constructing nano-heterojunction of MOFs with crystal regrowth for efficient degradation of tetracycline under visible light. *J. Alloys Compounds.* **904**, 164061 (2022).
50. Guo, C. *et al.* Copper-based polymer-metal–organic framework embedded with Ag nanoparticles: Long-acting and intelligent antibacterial activity and accelerated wound healing. *Chem. Eng. J.* **435**, 134915 (2022).
51. Lai, Q. *et al.* Two-dimensional Zr/Hf-hydroxamate metal–organic frameworks. *Chem. Commun.* https://doi.org/10.1039/d2cc00213b (2022).

52. Abdollahi, B., Farshnama, S., Abbasi Asl, E., Najafidoust, A. & Sarani, M. Cu(BDC) metal–organic framework (MOF)-based Ag_2CrO_4 heterostructure with enhanced solar-light degradation of organic dyes. *Inorg. Chem. Commun.* **138**, 109236 (2022).
53. Lv, S.-W. *et al.* Two novel MOFs@COFs hybrid-based photocatalytic platforms coupling with sulfate radical-involved advanced oxidation processes for enhanced degradation of bisphenol A. *Chemosphere* **243**, 125378 (2020).
54. Li, B., Zheng, J.-Q., Guo, J.-Z. & Dai, C.-Q. A novel route to synthesize MOFs-derived mesoporous dawsonite and application in elimination of Cu(II) from wastewater. *Chem. Eng. J.* **383**, 123174 (2020).
55. Li, H. *et al.* Enhanced adsorptive removal of anionic and cationic dyes from single or mixed dye solutions using MOF PCN-222. *RSC Adv.* **7**, 16273–16281 (2017).
56. Min, X. *et al.* Fe3O4@ZIF-8: A magnetic nanocomposite for highly efficient UO22+ adsorption and selective UO22+/Ln3+ separation. *Chem. Commun.* **53**, 4199–4202 (2017).
57. Ahmadijokani, F. *et al.* Ethylenediamine-functionalized Zr-based MOF for efficient removal of heavy metal ions from water. *Chemosphere* **264**, 128466 (2021).
58. Falcaro, P. *et al.* A new method to position and functionalize metal-organic framework crystals. *Nat. Commun.* **2**, 237 (2011).
59. Ricco, R., Malfatti, L., Takahashi, M., Hill, A. J. & Falcaro, P. Applications of magnetic metal–organic framework composites. *J. Mater. Chem. A* **1**, 13033 (2013).
60. Moon, H. R., Lim, D.-W. & Suh, M. P. Fabrication of metal nanoparticles in metal–organic frameworks. *Chem. Soc. Rev.* **42**, 1807–1824 (2013).
61. Khaletskaya, K. *et al.* Integration of porous coordination polymers and gold nanorods into core-shell mesoscopic composites toward light-induced molecular release. *J. Am. Chem. Soc.* **135**, 10998–11005 (2013).
62. Younas, M. *et al.* Recent progress and remaining challenges in post-combustion CO_2 capture using metal-organic frameworks (MOFs). *Progress Energy Combust. Sci.* **80**, 100849 (2020).
63. Shao, Y. *et al.* Magnetic responsive metal–organic frameworks nanosphere with core–shell structure for highly efficient removal of methylene blue. *Chem. Eng. J.* **283**, 1127–1136 (2016).
64. Nasiripur, P., Zangiabadi, M. & Baghersad, M. H. Visible light photocatalytic degradation of methyl parathion as chemical warfare agent's simulant via GO-Fe3O4/Bi2MoO6 nanocomposite. *J. Mol. Struct.* **1243**, 130875 (2021).
65. Seyfi, J. *et al.* Developing antibacterial superhydrophobic coatings based on polydimethylsiloxane/silver phosphate nanocomposites: Assessment of surface morphology, roughness and chemistry. *Progress Org. Coatings.* **149**, 105944 (2020).
66. Ahady, H., Taheri, R. A., Baghersad, M. H. & Kamali, M. Molecular dynamics simulation of bis(2-chloroethyl) sulfide gas separation by metal-organic and porous aromatic frameworks. *Microporous Mesoporous Mater.* **306**, 110402 (2020).
67. Yang, Q. *et al.* Fabrication of core-shell Fe3O4@MIL-100(Fe) magnetic microspheres for the removal of Cr(VI) in aqueous solution. *J. Solid State Chem.* **244**, 25–30 (2016).
68. Habibi, A., Baghersad, M. H., Bilabary, M. & Valizadeh, Y. Dithioates of Meldrum's acid, dimedone, and barbituric acid, novel sulfur transfer reagents for the one-pot copper-catalyzed conversion of aryl iodides into diaryl disulfides. *Tetrahedron Lett.* **57**, 559–562 (2016).
69. Abdel Maksoud, M. I. A. *et al.* Insight on water remediation application using magnetic nanomaterials and biosorbents. *Coordination Chem. Rev.* **403**, 213096 (2020).
70. Osman, A. I., Hefny, M., Abdel Maksoud, M. I. A., Elgarahy, A. M. & Rooney, D. W. Recent advances in carbon capture storage and utilisation technologies: A review. *Environ. Chem. Lett.* https://doi.org/10.1007/s10311-020-01133-3 (2020).
71. Huo, S.-H. & Yan, X.-P. Facile magnetization of metal–organic framework MIL-101 for magnetic solid-phase extraction of polycyclic aromatic hydrocarbons in environmental water samples. *Analyst* **137**, 3445 (2012).
72. Meteku, B. E. *et al.* Magnetic metal–organic framework composites for environmental monitoring and remediation. *Coordination Chem. Rev.* **413**, 213261 (2020).
73. Falcaro, P. *et al.* Dynamic control of MOF-5 crystal positioning using a magnetic field. *Adv. Mater.* **23**, 3901–3906 (2011).
74. Zhang, C.-F. *et al.* A novel magnetic recyclable photocatalyst based on a core–shell metal–organic framework Fe3O4@MIL-100(Fe) for the decolorization of methylene blue dye. *J. Mater. Chem. A* **1**, 14329 (2013).
75. Wang, Y., Xie, J., Wu, Y. & Hu, X. A magnetic metal-organic framework as a new sorbent for solid-phase extraction of copper(II), and its determination by electrothermal AAS. *Microchim. Acta* **181**, 949–956 (2014).
76. Qian, J.-J. *et al.* Fabrication of magnetically separable fluorescent terbium-based MOF nanospheres for highly selective trace-level detection of TNT. *Dalton Trans.* **43**, 3978 (2014).
77. Ke, F., Qiu, L.-G., Yuan, Y.-P., Jiang, X. & Zhu, J.-F. Fe3O4@MOF core–shell magnetic microspheres with a designable metal–organic framework shell. *J. Mater. Chem.* **22**, 9497 (2012).
78. Ke, F., Qiu, L.-G. & Zhu, J. Fe3O4@MOF core–shell magnetic microspheres as excellent catalysts for the Claisen-Schmidt condensation reaction. *Nanoscale* **6**, 1596–1601 (2014).
79. Li, G. L., Möhwald, H. & Shchukin, D. G. Precipitation polymerization for fabrication of complex core–shell hybrid particles and hollow structures. *Chem. Soc. Rev.* **42**, 3628 (2013).
80. Feng, L., Wang, K.-Y., Powell, J. & Zhou, H.-C. Controllable synthesis of metal-organic frameworks and their hierarchical assemblies. *Matter* **1**, 801–824 (2019).
81. Krawczyk, H. The stilbene derivatives, nucleosides, and nucleosides modified by stilbene derivatives. *Bioorg. Chem.* **90**, 103073 (2019).
82. Doddamani, R. V., Tasaganva, R. G., Inamdar, S. R. & Kariduraganavar, M. Y. Synthesis of chromophores and polyimides with a green chemistry approach for second-order nonlinear optical applications. *Polym. Adv. Technol.* **29**, 2091–2102 (2018).
83. Tsai, C.-Y. *et al.* Magnetically controllable random lasers. *Adv. Mater. Technol.* **2**, 1700170 (2017).
84. Qin, X. *et al.* Stilbene-benzophenone dyads for free radical initiating polymerization of methyl methacrylate under visible light irradiation. *Dyes Pigm.* **132**, 27–40 (2016).
85. Likhtenshtein, G. I. Stilbene molecular probes as potential materials for bioengineering: Real time analysis of antioxidants and nitric oxide, immunoassay in solution and biomembranes fluidity. *Adv. Mater. Res.* **699**, 718–723 (2013).
86. Roloff, A., Nelles, D. A., Thompson, M. P., Yeo, G. W. & Gianneschi, N. C. Self-transfecting micellar RNA: Modulating nanoparticle cell interactions via high density display of small molecule ligands on micelle coronas. *Bioconjug. Chem.* **29**, 126–135 (2017).
87. Rao, R. N., Venkateswarlu, N., Khalid, S., Narsimha, R. & Sridhar, S. Use of solid-phase extraction, reverse osmosis and vacuum distillation for recovery of aromatic sulfonic acids from aquatic environment followed by their determination using liquid chromatography-electrospray ionization tandem mass spectrometry. *J. Chromatogr. A* **1113**, 20–31 (2006).
88. Rao, R. N., Venkateswarlu, N., Khalid, S. & Narsimha, R. LC-PDA and LC-ESI-MS separation and determination of process-related substances arising from stilbene-type fluorescent whitening agents. Application to monitoring of their photodegradation products in industrial effluents and aqueous environmental systems. *J. Separation Sci.* **28**, 443–452 (2005).
89. DeCoste, J. B. *et al.* Stability and degradation mechanisms of metal–organic frameworks containing the Zr6O4(OH)4 secondary building unit. *J. Mater. Chem. A* **1**, 5642 (2013).
90. Kandiah, M. *et al.* Synthesis and stability of tagged UiO-66 Zr-MOFs. *Chem. Mater.* **22**, 6632–6640 (2010).
91. Wu, H., Yildirim, T. & Zhou, W. Exceptional mechanical stability of highly porous zirconium metal-organic framework UiO-66 and its important implications. *J. Phys. Chem. Lett.* **4**, 925–930 (2013).

92. Schaate, A. *et al.* Modulated synthesis of Zr-based metal-organic frameworks: From nano to single crystals. *Chem. Eur. J.* **17**, 6643–6651 (2011).
93. Guillerm, V. *et al.* A series of isoreticular, highly stable, porous zirconium oxide based metal-organic frameworks. *Angew. Chem. Int. Ed.* **51**, 9267–9271 (2012).
94. Huang, Y., Qin, W., Li, Z. & Li, Y. Enhanced stability and CO_2 affinity of a UiO-66 type metal–organic framework decorated with dimethyl groups. *Dalton Trans.* **41**, 9283 (2012).
95. Cavka, J. H. *et al.* A new zirconium inorganic building brick forming metal organic frameworks with exceptional stability. *J. Am. Chem. Soc.* **130**, 13850–13851 (2008).
96. Valenzano, L. *et al.* Disclosing the complex structure of UiO-66 metal organic framework: A synergic combination of experiment and theory. *Chem. Mater.* **23**, 1700–1718 (2011).
97. Ahmadipouya, S. *et al.* Magnetic Fe3O4@UiO-66 nanocomposite for rapid adsorption of organic dyes from aqueous solution. *J. Mol. Liq.* **322**, 114910 (2021).
98. Abid, H. R. *et al.* Nanosize Zr-metal organic framework (UiO-66) for hydrogen and carbon dioxide storage. *Chem. Eng. J.* **187**, 415–420 (2012).
99. Lv, S.-W. *et al.* Fabrication of Fe3O4@UiO-66-SO3H core–shell functional adsorbents for highly selective and efficient removal of organic dyes. *New J. Chem.* **43**, 7770–7777 (2019).
100. Zhao, H.-X. *et al.* Theranostic metal–organic framework core–shell composites for magnetic resonance imaging and drug delivery. *Chem. Sci.* **7**, 5294–5301 (2016).
101. Moghaddam, F. M., Saberi, V., Kalhor, S. & Ayati, S. E. A novel highly dispersive magnetic nanocatalyst in water: Glucose as an efficient and green ligand for the immobilization of copper(ii) for the cycloaddition of alkynes to azides. *RSC Adv.* **6**, 80234–80243 (2016).
102. Moghaddam, F. M., Saberi, V., Kalhor, S. & Veisi, N. Palladium(II) immobilized onto the glucose functionalized magnetic nanoparticle as a new and efficient catalyst for the one-pot synthesis of benzoxazoles. *Appl. Organometal. Chem.* **32**, e4240 (2018).

Author contributions

M.H.B. is a assistant proffessor of organic chemistry. He devised the project and the main conceptual ideas and was in charge of overall direction and planning. M.R.K. is a Assistant proffessor of organic chemistry in Applied Biotechnology Research Center in Baqiyatallah University of Medical Sciences . He performed the experiments, analyzed spectra, and wrote the original draft. All authors reviewed the manuscript.

Competing interests

The authors declare no competing interests.

Additional information

Correspondence and requests for materials should be addressed to M.H.B.

Reprints and permissions information is available at www.nature.com/reprints.

Publisher's note Springer Nature remains neutral with regard to jurisdictional claims in published maps and institutional affiliations.